doi:10.1093/brain/awt146 Brain 2013: 136; 2239–2252 | 2239

BRAIN
A JOURNAL OF NEUROLOGY

In vivo characterization of the early states of the amyloid-beta network

Jorge Sepulcre,[1,2] Mert R. Sabuncu,[2,3] Alex Becker,[1] Reisa Sperling[2,4,5] and Keith A. Johnson[1,4,5]

1 Division of Nuclear Medicine and Molecular Imaging, Department of Radiology, Massachusetts General Hospital and Harvard Medical School, Boston, MA, USA
2 Athinioula A. Martinos Centre for Biomedical Imaging, Charlestown, MA, USA
3 Computer Science and Artificial Intelligence Lab, Massachusetts Institute of Technology, Cambridge, MA, USA
4 Centre for Alzheimer Research and Treatment, Department of Neurology, Brigham and Women's Hospital and Harvard Medical School, Boston, MA, USA
5 Department of Neurology, Massachusetts General Hospital and Harvard Medical School, Boston, MA, USA

Correspondence to: Jorge Sepulcre,
Division of Nuclear Medicine and Molecular Imaging,
Department of Radiology,
Massachusetts General Hospital and Harvard Medical School,
Boston, MA, USA
E-mail: sepulcre@nmr.mgh.harvard.edu

Correspondence may also be addressed to: Keith A. Johnson, E-mail: kajohnson@pet.mgh.harvard.edu

Alzheimer's disease is a neurodegenerative disease that is associated with the abnormal accumulation of amyloid-β. Much is known about regional brain atrophy in Alzheimer's disease, yet our knowledge about the network nature of Alzheimer's disease-associated amyloid-β accumulation is limited. We use stepwise connectivity analysis of Pittsburgh Compound B positron emission tomography images to reveal the network properties of amyloid-β deposits in normal elderly subjects and clinical patients with Alzheimer's disease. We found that amyloid-β accumulation in the medial temporal lobe is associated with accumulation in cortical regions such as orbitofrontal, lateral temporal and precuneus/posterior cingulate cortices in Alzheimer's disease. In normal subjects, there was a predominant association between amyloid-β deposits in the hippocampus and the midline prefrontal/orbitofrontal regions, even in those with very low amyloid-β burden. Moreover, the orbitofrontal cortex, amygdala nucleus and hippocampus exhibit hub properties in the amyloid-β network that may be critical to understanding the putative spreading mechanisms of Alzheimer's disease pathology in early stages.

Keywords: Alzheimer's disease; network; amyloid; graph theory; early stages

Abbreviations: HFPG = hippocampal formation and parahippocampal gyrus; PIB = Pittsburgh compound B

Introduction

Alzheimer's disease is a devastating neurological illness characterized by misfolded proteins that progressively accumulate as intracellular neurofibrillary tangles (Mann, 1985; Arnold *et al*., 1991; Braak and Braak, 1991*a*, *b*) and insoluble self-aggregating amyloid-β in extracellular space (Ogomori *et al*., 1989; Braak and Braak, 1991*b*; Mattson, 2004; Walsh and Selkoe, 2004; Selkoe, 2006; Ikonomovic *et al*., 2008; Hyman *et al*., 2012). The brain neurofibrillary tangle and amyloid-β deposits are not randomly distributed but have characteristic spatial patterns (Hyman *et al*., 1984; Lewis *et al*., 1987; Braak *et al*., 1989, 2006; Kalus *et al*.,

Received January 9, 2013. Revised April 23, 2013. Accepted April 29, 2013

1989; Arnold *et al*., 1991; Braak and Braak, 1991*b*; Thal *et al*., 2002). For instance, in early stages of the evolution of Alzheimer's disease pathology neurofibrillary tangles are frequently located in the trans-entorhinal cortex, and amyloid-β in neocortical regions, particularly in basal regions of temporal and frontal lobe (Braak and Braak, 1991*b*; Thal *et al*., 2002; Braak *et al*., 2006). When Alzheimer's disease is well established, both neuropathology landmarks largely affect a set of distinctive brain regions now considered to be cortical hubs, which include the default mode network (Buckner *et al*., 2009; Sepulcre *et al*., 2010).

During the past decades, Alzheimer's disease research has particularly focused on describing the early stages of the disease with the hope of implementing preventive treatments with disease-modifying agents. The introduction of molecular imaging techniques such as PET with Pittsburgh compound B (PIB-PET) has facilitated early detection by allowing the *in vivo* visualization of brain amyloid-β deposition (Klunk *et al*., 2001, 2004; Bacskai *et al*., 2003; Nordberg, 2004). However, PIB-PET imaging, as well as previous pathological studies, have also brought new challenges. For instance, large numbers of elderly cognitively normal subjects have significant amyloid-β deposits detected by PIB-PET (10–50%) (Lopresti *et al*., 2005; Mintun *et al*., 2006; Kemppainen *et al*., 2007; Rowe *et al*., 2007; Forsberg *et al*., 2008; Gomperts *et al*., 2008; Rentz *et al*., 2010) suggesting an early onset and continuous nature of the pathology (Vlassenko *et al*., 2011). Another challenge is that although Alzheimer's disease has been recognized as a disorder of large-scale brain systems, it has often been studied by focusing on a single vulnerable region (or multiple unrelated regions). The reason for regional focus in such studies was, in part, an issue of practicality; however, it also has to do with the limitations of techniques for surveying distributed brain systems. This outlook has changed in recent years. For instance, with the development of functional and structural connectivity MRI and graph theory based methods we now know that, rather than appearing in functionally unrelated regions, neurodegeneration in Alzheimer's disease occurs within the boundaries of well-known functional/structural connectivity networks (Gusnard and Raichle, 2001; Greicius *et al*., 2004; Greicius, 2008; Buckner *et al*., 2009; Seeley *et al*., 2009; Zhou *et al*., 2012).

Other evidence that supports the idea of Alzheimer's disease as a network pathology is the 'synaptic excitatory toxicity hypothesis' (Mackenzie and Miller, 1994; Gouras *et al*., 1997; Palop *et al*., 2006; Palop and Mucke, 2010). This hypothesis states that neural damage can be the result of the over-activation of *N*-methyl-D-aspartic acid receptors by glutamate at the synaptic level. Consequently, interconnected regions with high basal metabolism, and presumably high excitatory synaptic activity, could be the target for a progressive neurodegenerative cascade. It has been demonstrated in experimental settings that the processing of amyloid precursor protein and increasing of amyloid peptides in the extracellular space depends on synaptic activity (Nitsch *et al*., 1993; Kamenetz *et al*., 2003; Cirrito *et al*., 2005; Selkoe, 2006; Brody *et al*., 2008; Bero *et al*., 2011). In this sense, the overlap between functionally highly connected cortical hubs and amyloid-β deposits, as well as regions with elevated aerobic glycolysis metabolism, suggest that continuously sustained activity may lead to consecutive activity-dependent neurodegeneration (Hardy, 1992; Hardy and Higgins, 1992; Mintun *et al*., 2006; Selkoe, 2006; Bero *et al*., 2012).

In this study, we aim to investigate the *in vivo* amyloid-β spatial co-variation patterns during normal ageing to understand the distributed systems affected in preclinical stages of Alzheimer's disease. We postulate that amyloid-β deposits are not independent between specific regions, even when they are far away, reflecting the neurodegeneration influence of interconnected neurons at the network level. More specifically, we think that it is the regional co-variation rather than the total amount of amyloid-β accumulation—known to be relatively sparse in some regions of the medial temporal lobe—that will elucidate pathological features of Alzheimer's disease genesis. In other words, we hypothesize that the amyloid-β co-variation between pathological deposits in the medial temporal lobe and other parts of the brain will reveal the early stages of the amyloid-β network. We use graph theory techniques and *in vivo* PIB-PET imaging to characterize the spatial associations, stepwise connectivity and network stages of amyloid-β brain deposits in the ageing brain.

Materials and methods

Participants

Table 1 shows the demographics of elderly subjects and the participants with Alzheimer's disease. Forty cognitively normal older adults and 30 patients with Alzheimer's disease were included in the primary analysis of the study. Participants were recruited from ongoing neuroimaging longitudinal studies in ageing and during screening for dementia clinical trials at the Massachusetts General and Brigham and

Table 1 Participant demographic

	Alzhemier's disease	Elderly control subjects	Elderly control subjects low PIB
Sample size	30 (13 male)	40 (14 male)	20 (6 male)
Mean age, years (SD)	73.03 (7.99)	76.15 (8.04)	73.47 (9.38)
Mean education, years (SD)	17.5 (1)	16.24 (2.88)	16.5 (3.22)
Mean MMSE (SD)	25 (1.63)	29.05 (1.1)	28.83 (1.33)
Mean CDR	1	0	0
PIB −/+	0/30	20/20	20

MMSE = Mini-Mental State Examination; CDR = clinical dementia rating; PIB −/+ = elderly control subjects with mean cortical PIB distribution volume ratio $\leqslant 1.15$ or > 1.1.

Women's Hospitals. All elderly controls and participants with Alzheimer's disease were studied using protocols and informed consent procedures approved by the Partners Human Research Committee. Inclusion as a cognitively normal elderly subject required a normal neurological examination, a clinical dementia rating (Hughes *et al*., 1982; Morris, 1993) scale score of 0, a Mini-Mental State Examination >27 and performance within 1.5 SD on age and education-adjusted norms on cognitive testing (Becker *et al*., 2011). Moreover, none of the cognitively normal elderly participants had any notable medical or neuropsychiatric illness, and none had a history of alcoholism, drug abuse, or head trauma, or a family history of autosomal dominant Alzheimer's disease. All participants with Alzheimer's disease were Clinical Dementia Rating scale = 1 and satisfied criteria for a clinical diagnosis of probable Alzheimer's disease according to the National Institute of Neurological and Communicative Disorders and Stroke/Alzheimer's Disease and Related Disorders Association criteria (McKhann *et al*., 1984). Elderly controls and Alzheimer's disease subjects underwent a standard battery of neuropsychological tests (Becker *et al*., 2011). In addition to the primary analysis of neuroimaging data, 20 subjects of the elderly controls sample, classified as low amyloid-β burden subjects (see below for details), were analysed 1 year after their recruitment (~10–13 months).

We further validated that PIB network follows functional pathways by using a functional connectivity MRI data set from 100 normal young control subjects (mean age = 21.3 years, 37 male). Young control subjects were obtained from a neuroimaging collaborative effort across multiple laboratories at Harvard and at the Massachusetts General Hospital (Yeo *et al*., 2011). These subjects met the following criteria: their functional MRI data exhibited a signal-to-noise ratio >100, no artefacts were detected in the magnetic resonance data, the subjects had no self-reported neurological and psychiatric disease and psychoactive medication history. All young control participants provided written informed consent in accordance with the Declaration of Helsinki and guidelines set by institutional review boards of Harvard University or Partners Healthcare.

Finally, two more data sets were included in the study in order to replicate our findings. First, we analysed 20 new subjects with Alzheimer's disease to assess the potential influence of volume atrophy in our approach (mean age = 71.32 years, eight male, Clinical Dementia Rating scale = 1). We also analysed an independent data set of 20 elderly PIB-negative control subjects (mean age = 71.23 years, eight male). These new subjects were also recruited from ongoing neuroimaging longitudinal studies at the Massachusetts General and Brigham and Women's Hospitals and this recruitment followed the protocols, selection criteria and informed consent procedures as stated above.

Pittsburgh compound B positron emission tomography acquisition procedures in elderly controls and subjects with Alzheimer's disease

We used PET with a ^{11}C-PIB, [*N*-methyl ^{11}C-2-(4-methylaminophenyl)-6-hydroxybenzothiazole] imaging tracer that specifically binds to fibrillar amyloid-β (Mathis *et al*., 2002; Bacskai *et al*., 2003). Procedures for PIB–PET imaging have been described previously (Mathis *et al*., 2003; Klunk *et al*., 2004; Johnson *et al*., 2007); data were acquired at Massachusetts General Hospital on a Siemens/CTI ECAT PET HR scanner. Following a transmission scan, 10–15 mCi ^{11}C-PIB was injected intravenously as a bolus and followed immediately by a 60-min dynamic PET scan in 3D mode (63 image planes, 15.2 cm axial field of view, 5.6 mm transaxial resolution and 2.4 mm slice interval; 69 frames: 12 × 15 s, 57 × 60 s). PIB retention was expressed as the distribution volume ratio at each voxel, applying Logan's graphical method with time-activity data acquired over 60 min after tracer injection (Lopresti *et al*., 2005; Mintun *et al*., 2006; Johnson *et al*., 2007) and using the cerebellar cortex as reference region (Logan *et al*., 1990). Participants were classified as PIB-negative—also referred here as low amyloid burden—and PIB-positive subjects by using the average PIB distribution volume ratio intensity in frontal, lateral parietal and lateral temporal, and retrosplenial cortices (the FLR region) (Hedden *et al*., 2009). Mean FLR distribution volume ratio <1.15 was used as cut-off for PIB-negative classification. Corrections for non-uniformity of detector response, dead time, random coincidences, scattered radiation and attenuation were performed (Hedden *et al*., 2009). In addition, each subject's PIB-PET data were spatially normalized to the MNI atlas space and smoothed with a Gaussian filter (8-mm full-width at half-maximum) using Statistical Parametric Mapping (SPM2; Wellcome Department of Cognitive Neurology). For computational efficiency we down-sampled all PIB neuroimaging data to 8 mm isotropic voxels. Finally, as part of the imaging protocol we acquired high-resolution MRI images from all participants using magnetization-prepared rapid gradient-echo (MPRAGE) images as described in Hedden *et al*. (2009).

Functional connectivity acquisition procedures in young control participants

Image acquisition was performed on a 3 T Tim Trio system (Siemens) using a 12-channel phased-array head coil with a functional gradient-echo echo-planar pulse sequence sensitive to blood oxygen level-dependent contrast (repetition time = 2500 ms, echo time = 30 ms, flip angle = 90°, 3.0 mm isotropic voxels, 148 time points). An optimized functional connectivity MRI protocol (Van Dijk *et al*., 2010), extending from the approach developed by Biswal *et al*. (1995) was used in the preprocessing steps. The first four volumes were removed to allow for T_1-equilibration effects, followed by compensation of systematic, slice-dependent time shifts, motion correction and normalization to the atlas space of the MNI (SPM2, Wellcome Department of Cognitive Neurology, London, UK). Temporal filtering removed constant offsets and linear trends over each run while retaining frequencies <0.08 Hz. Several sources of spurious or regionally non-specific variance were removed by regression of nuisance variables including: six parameter rigid body head motion (obtained from motion correction), signal averaged over the whole brain, signal averaged over the lateral ventricles, and signal averaged over a region centred in the deep cerebral white matter (Biswal *et al*., 1995; Birn *et al*., 2006; Van Dijk *et al*., 2010). Finally, for computational efficiency we down-sampled all functional connectivity MRI neuroimaging data to 8 mm isotropic voxels.

Stepwise connectivity analysis

Stepwise connectivity analysis is a graph theory-based method that complements neuroimaging conventional connectivity approaches by detecting not only direct spatial correlations between brain regions but also multistep associations between a given region and the rest of the brain through relay stations (Sepulcre *et al*., 2012*b*). In this sense, stepwise connectivity facilitates a more comprehensive description of the spatial regional associations, for example in the amyloid network. Before the stepwise connectivity network analysis, we performed the

following steps using the PIB distribution volume ratio maps: (i) to compute the group-based correlations, we first extracted each individual subject's image data within a whole brain mask (3329 voxels), vectorized these data and stacked them up into a 'PIB intensity' matrix where the rows represented the voxels and the columns corresponded to subjects (Fig. 1A); (ii) next, we computed the Pearson R, or product-moment correlation coefficient between each voxel pair, which yielded a 3329 × 3329 'PIB association matrix', where only positive correlations were saved; (iii) we built the group-specific whole-brain networks using a false discovery rate (FDR; Benjamini and Hochberg, 1995) correction at 0.001 level to control for the rate of false positives in the final group-specific network adjacency matrices (Fig. 1B). Therefore, only FDR corrected correlations were included in the final analysis; and (iv) we binarized the resulting matrices to obtain undirected and unweighted data that served as input data for the stepwise connectivity analysis.

An additional analysis was performed to check the potential influence of volume atrophy in our approach. We used SPM2 (Wellcome Department of Cognitive Neurology) to compute a spatial normalization and segmentation of the individual high-resolution MPRAGE MRI sequences using the voxel-based morphometry protocol. We then computed the partial correlations ($P < 0.001$) between the 'PIB intensity' values of each voxel, while controlling for the grey matter concentration values at the corresponding voxel pair computed by SPM2. Finally, the stepwise connectivity analysis with atrophy correction followed the same steps as the original stepwise connectivity analysis that did not correct for atrophy.

A similar protocol was performed for the functional connectivity MRI data in the young control sample but instead of the 'PIB association matrix', a subject level functional connectivity matrix was obtained from resting state blood oxygen level-dependent series (functional connectivity MRI association matrix).

Stepwise connectivity analysis aims to characterize regions that connect to specific target areas at different levels of 'link-step' distances (e.g. Fig. 1Ba and Bc) (Sepulcre *et al*., 2012*b*). In our framework, a step refers to the number of links that belong to a path

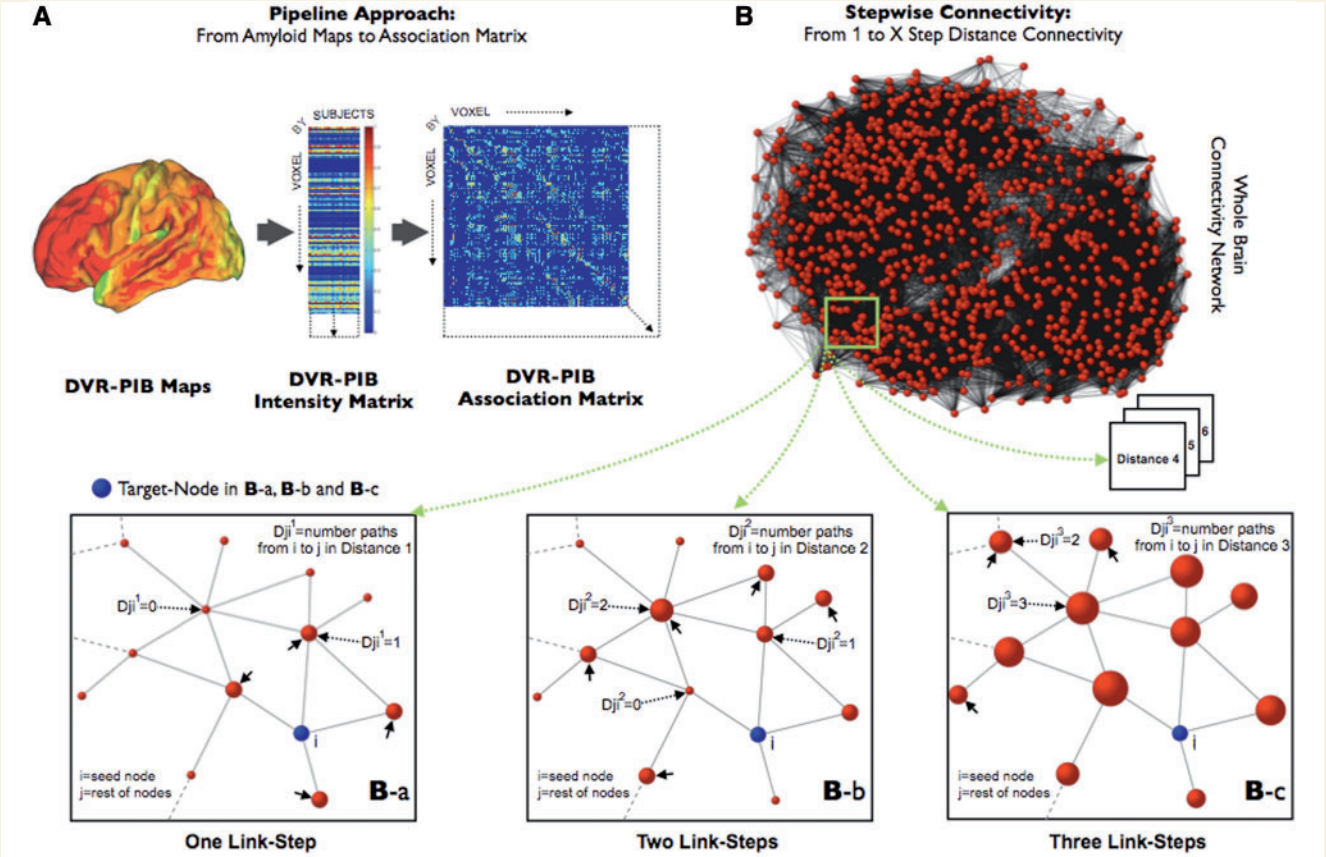

Figure 1 Stepwise connectivity method in PIB-PET images. (**A**) Main steps of the pipeline approach of the study, from conventional PIB images to association matrix. ^{11}C-PIB PET images, transformed to distribution volume ratio maps (DVR), were used to obtain group-level intensity matrices (voxels × subjects). Later, group-specific association matrices were calculated by applying the Pearson R correlation coefficient between all pair of voxels. Finally, we use the association matrices to achieve FDR corrected adjacency matrices and build the specific graphs for each study group. (**B**) Simplified diagram of the stepwise connectivity (SC) method [figure partially adapted from Sepulcre *et al*. (2012*b*)]. Stepwise connectivity analysis takes advantage of the whole connectivity association matrix and analyses the connectivity patterns of target regions using a wide range of link-step distances. Briefly, from any node (j; red nodes) in the brain, we compute the number of pathways that connect to a voxel in an *a priori* target node (i; blue node) with a particular number of links *l* (D_{ji}^{l} where *l* is the specific link-step distance). In the 'One Link-Step' case, only direct connections to the target are considered (small arrows in **Ba**). In higher order step distances, connectivity patterns beyond direct connections are obtained (**Bb** and **c**). Note that for schematic purposes only one target voxel-node (blue colour) is displayed in **Ba–c**.

connecting a node to the target area. The degree of stepwise connectivity of a voxel j for a given step distance l (D_{ji}^{l} in Fig. 1B) is computed from the count of all paths that: (i) connect voxel j to any voxel in target area i; and (ii) have an exact length of l.

Therefore in the stepwise connectivity analysis of specific targets, the value D_{ji}^{l} of a brain voxel represents the sum of the number of pathways between that voxel and any of the voxels in the target region in a given link-step distance. Note also that in stepwise connectivity analysis there is no discrimination between the contributions of local and long-range connections since physical distances play no role in the computations.

In this study, we were interested in the spatial correlations between the medial temporal lobe, specifically hippocampal formation and parahippocampal gyrus (HFPG), and the rest of the brain, and in particular the core of the default mode network, namely the posterior cingulate cortex. It has been suggested that interactions between distant brain systems, such as the medial temporal structures and the cingulate cortex, may be the key factor to conceptualizing the conversion from MCI to Alzheimer's disease stages (Tosun *et al*., 2011). HFPG and posterior cingulate cortex are key regions that exhibit early and profound neurodegeneration in Alzheimer's disease and we selected them as representing the medial temporal and the distributed brain degeneration, respectively. We selected *a priori* Anatomical Automatic Labeling regions of interest (Tzourio-Mazoyer *et al*., 2002) as target areas. Although left and right regions of interest were used in the analyses of the study, we observed no salient lateralization in our results and thus only left hemisphere results from left regions of interest are presented to avoid redundancy.

We note that since no directionality information is present in the (PIB or functional connectivity MRI) association matrix data, we decided not to impose any restrictions about recurrent pathways crossing the target regions multiple times in the stepwise connectivity analyses. On the other hand, an important aspect of the stepwise connectivity approach is that the interpretation of the number of link-steps depends heavily on the resolution of the images. Therefore, we explored a wide range of link-step distances in order to characterize the stability of the derived maps. As seen in Supplementary Fig. 1, the PIB-related stepwise connectivity patterns are topographically stable after three to four link-steps. The cortical map of this final stable state collapses onto regions previously described as the cortical hubs of the human brain (Buckner *et al*., 2009; Sepulcre *et al*., 2010). Therefore, in the 'Results' section we only show maps up to three steps. Finally, similar to the usage of functional connectivity in resting state functional MRI, we adopt the term 'amyloid network connectivity' or connectivity in general to refer to the degree of association (reflected in stepwise connectivity patterns) between the amyloid load of distinct brain regions; and not as a direct structural or axonal connectivity concept.

The statistical assessment of the 1-year longitudinal stepwise connectivity changes of HFPG in the 20 elderly controls with low amyloid-β burden was carried out using a permutation test. We obtained the null hypothesis distribution for comparing the stepwise connectivity baseline and follow-up differences by randomly swapping the temporal ordering of the scans and creating 10 000 simulated data sets. We then computed the adjacency matrix for each data set and repeated the stepwise connectivity analysis for these simulated 'baseline' and '1 year follow-up' scans, separately. Next, we computed the longitudinal difference between stepwise connectivity measures by subtracting the '1-year follow-up' values from the 'baseline' values. These differences were finally compared with the actual differences obtained with the true baseline versus follow-up data sets to obtain a permutation P-value for each measure (significance level permutation $P < 0.05$ are reported).

Interconnectors between target areas

Stepwise connectivity analysis allows us to explore the main streams of connectivity between a target region and the rest of the brain. A complementary method to this approach is what we call the interconnector analysis, which aims to characterize the relationship between two target regions of interest (Sepulcre *et al*., 2012*b*). Here, we are interested in using this approach to capture the direct interconnectors between pairs of regions, such as HFPG and posterior cingulate cortex.

First, we detect interconnector voxels (nodes), which are the voxels that have direct connectivity, i.e. connectivity at one link-step, to multiple target regions. Then, we compute the degree of connectivity of a given interconnector node, by summing the total number of paths to the target nodes. In summary, this interconnector analysis strategy provides direct information about the interface regions that bond together two target regions in the brain (Sepulcre *et al*., 2012*b*).

Degree centrality (network hubs)

Degree centrality, a classical graph theoretic measure, is defined for each node (voxel) as the total number of its links to the rest of the nodes in the graph. Degree centrality quantifies 'network hubs' and has been used to reveal cortical hubs based on resting state functional connectivity MRI data (Buckner *et al*., 2009; Sepulcre *et al*., 2010). In this work, we used the degree centrality method to further identify the network hubs of the graph in the elderly controls with low amyloid-β burden. Note that degree centrality relates to the number of connections of a node to the rest of the network nodes, while the stepwise connectivity degree of connectivity at 1-step distance measures the number of connections between all nodes in a given region of interest and the rest of the network nodes. Therefore, both metrics share similarities but represent different pieces of information.

Visualization

As a final step, all resulting maps were projected onto the cerebral hemispheres of the PALS surface (PALS-B12) provided with Caret software (Van Essen and Dierker, 2007) using the 'enclosing voxel algorithm' and 'multi-fiducial mapping' settings. To aid visualization across different link-step conditions, all surface stepwise connectivity images were displayed using a normalized colour scale from 0 to 1, where 0 is the intensity corresponding to z-score equal to zero and 1 is the maximum z-score in the image. We used Pajek software (de Nooy *et al*., 2005) and Kamada-Kawai energy layout (Kamada and Kawai, 1989) for the network graph display in Fig. 4. The Kamada-Kawai algorithm is a force layout method based on a network energy procedure that arranges the nodes in a network by minimizing the length and crossing of links. It assigns forces in the links and nodes of the network and finds the optimal lengths and positions of them. We visually represented degree centrality (degree of connectivity) by plotting regions with higher values as larger nodes.

Results

Amyloid-β deposition in the medial temporal lobe and distributed regions of the cortex are correlated in Alzheimer's disease

Our stepwise connectivity analysis of HFPG in Alzheimer's disease reveals strong direct correlations with three distributed cortical regions: orbitofrontal, anterior-lateral temporal and precuneus/posterior cingulate cortex cortices (one link-step map to HFPG; Fig. 2Aa–c). Amyloid-β deposit in HFPG is also directly associated with amyloid-β all along the contralateral HFPG (detailed inset in Fig. 2A). Interestingly, the pattern of stepwise connectivity highlights the orbitofrontal, lateral temporal and precuneus regions in the next steps (two link-step map to HFPG; Fig. 2Ad–f) to finally reach a stable topology in which the midline prefrontal and large lateral prefrontal areas dominate the connectivity landscape (three link-step map to HFPG and beyond; Fig. 2Ag; and Supplementary Fig. 1). Stepwise connectivity maps with and without atrophy correction generate similar results in an independent data set (Supplementary Fig. 2).

To further examine the amyloid-β associations between HFPG and distributed cortical systems commonly affected in Alzheimer's disease, we used a network interconnector analysis that captures the direct links between HFPG and posterior cingulate cortex. Similar to the previous stepwise connectivity results, this analysis shows that there are mainly three regions that are placed inbetween HFPG and posterior cingulate cortex, in terms of amyloid-β accumulation (white circles nodes in Fig. 2B).

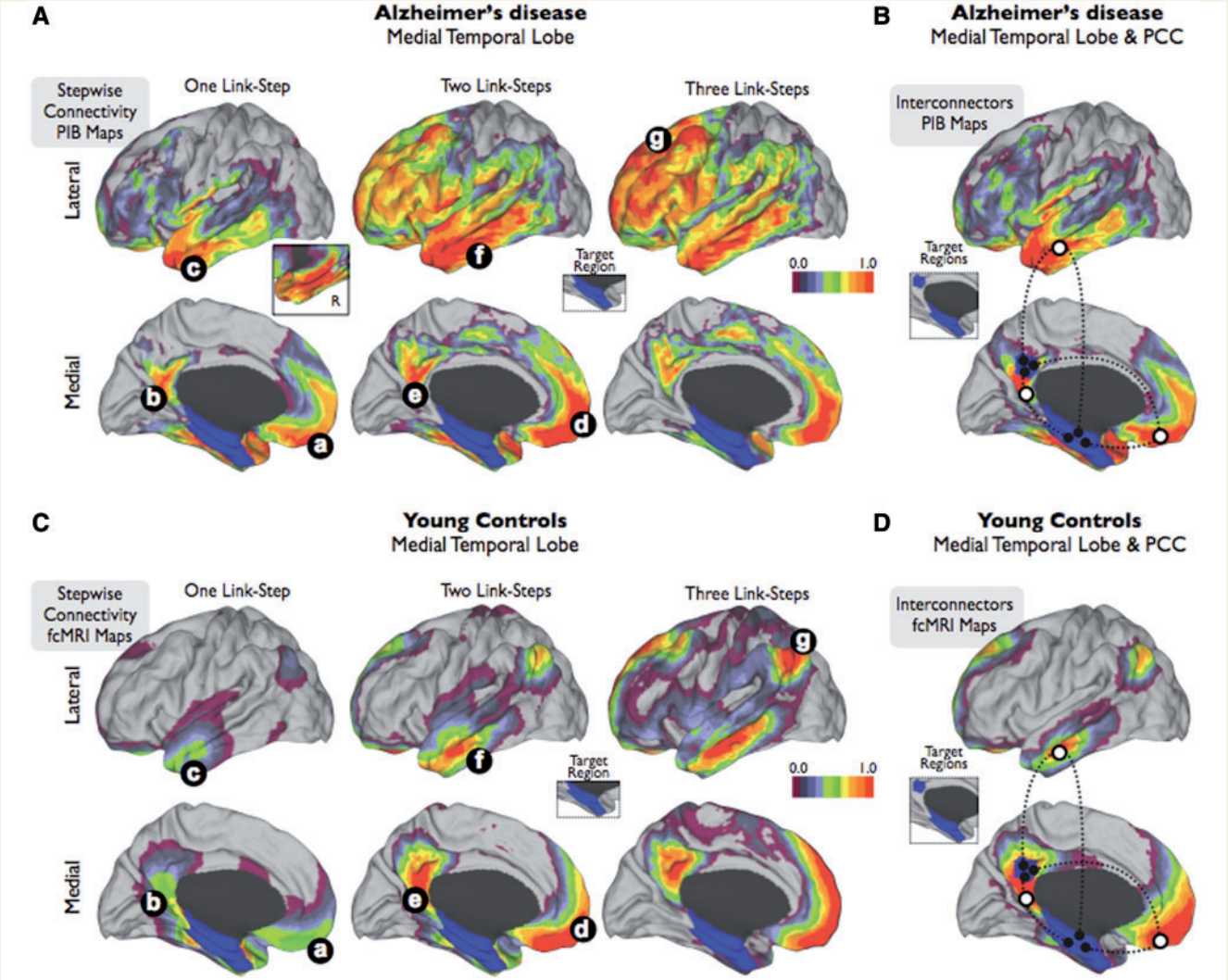

Figure 2 Stepwise connectivity analysis of medial temporal lobe and interconnector analysis of medial temporal lobe and posterior cingulate cortex in PIB-PET images of patients with Alzheimer's disease (**A** and **B**) and in functional connectivity MRI images of young controls (**C** and **D**). Inset in **A** shows the contralateral amyloid-β connectivity in one-step. Colour bars represent a normalized colour scale from 0 to 1, where 0 is the intensity corresponding to *z*-score equal to zero and 1 is the maximum *z*-score.

Finally, we performed an additional analysis to confirm that the stepwise connectivity patterns of amyloid-β deposits follow specific functional connectivity networks in the human brain. In order to do so, we used stepwise connectivity analysis on functional connectivity MRI data in a young control sample. In agreement with the amyloid-β spatial associations obtained in Alzheimer's disease, stepwise connectivity of functional connectivity images shows that orbitofrontal, lateral temporal and posterior cingulate cortex regions display direct connectivity with HFPG (one link-step map to HFPG; Fig. 2Ca–c). Subsequently, the functional stepwise connectivity pattern in further steps expands to the midline prefrontal, lateral temporal and precuneus/posterior cingulate cortex (two link-step map to HFPG; Fig. 2Cd–f) to finally reach the cortical hubs of the human brain. Although topological similarities between amyloid-β and functional connectivity maps are striking, two major divergences arise. On one hand, the functional connectivity in a large number of steps between distributed regions and HFPG involves a hub in the lateral parietal region in young controls (three link-step map to HFPG; Fig. 2Cg) that is conspicuously absent in the amyloid-β map of Alzheimer's disease. However, it is also worth noting that in the young controls, the connectivity between the medial temporal lobe and lateral parietal region is the least prominent among all possible pathways. On the other hand, the ventrolateral prefrontal region of the brain seems to be more pronounced in the amyloid-β map of patients with Alzheimer's disease, compared to the functional connectivity MRI maps in young controls. Similarly to the Alzheimer's disease maps, our interconnector analysis of functional connectivity MRI data revealed that HFPG and posterior cingulate cortex connectivity is achieved through three direct functional pathways; orbitofrontal, mid-lateral temporal and inferior precuneus/posterior cingulate cortex cortices (white circles in Fig. 2D).

Association between amyloid-β deposition in the medial temporal lobe and the midline prefrontal cortex in elderly controls

Stepwise connectivity analysis of HFPG in elderly controls reveals noticeable topological features. We found that amyloid-β in HFPG is preferentially associated with the midline prefrontal and orbitofrontal areas (one link-step map to HFPG; Fig. 3Aa and b). Compared with the Alzheimer's disease results, the association between the medial temporal lobe and orbitofrontal/midline prefrontal regions is more prominent than other potential connectivity patterns such as between medial temporal lobe and the lateral temporal or posterior cingulate cortex areas. In this group, amyloid-β deposits in HFPG are also directly associated with amyloid-β deposits in the contralateral hippocampus but not in the parahippocampus cortex (inset in Fig. 3A). The pattern of stepwise connectivity continues to connect to the orbitofrontal, midline and lateral prefrontal, lateral temporal and precuneus/posterior cingulate cortex (two and three link-step maps to HFPG; Fig. 3Ac–g) areas in later steps, which conforms to a similar map as the one obtained in the Alzheimer's disease group. In addition, the interconnector analysis confirms that midline prefrontal and orbitofrontal areas (white circle in Fig. 3B) intermediate the amyloid-β

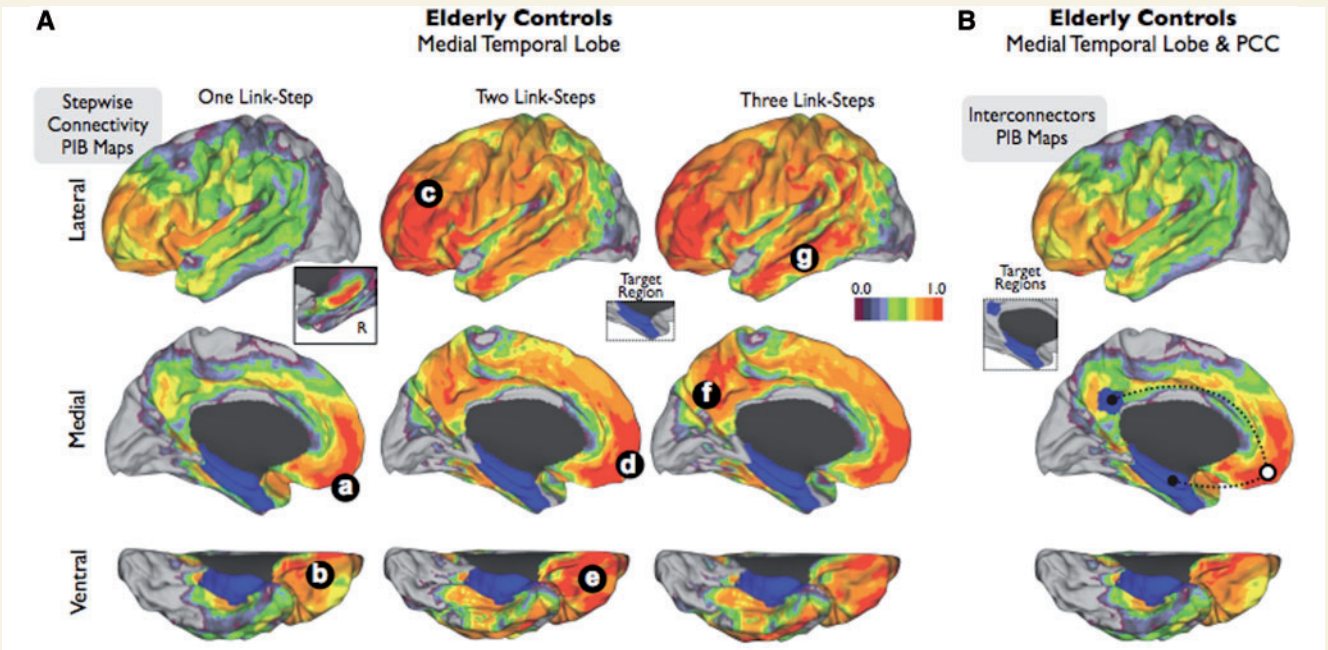

Figure 3 Stepwise connectivity analysis of medial temporal lobe (**A**) and interconnector analysis of medial temporal lobe and posterior cingulate cortex (**B**) in PIB-PET images of elderly controls. Inset in **A** shows the contralateral amyloid-β connectivity in one-step. Colour bar represents a normalized colour scale from 0 to 1, where 0 is the intensity corresponding to *z*-score equal to zero and 1 is the maximum *z*-score.

association between HFPG and the hubs of distributed systems such as the posterior cingulate cortex. Cortical maps displayed in Figs 2 and 3 use a relative threshold based on the maximal degree of stepwise connectivity of the group in order to reveal the topological patterns of association. Therefore, it may seem that the elderly controls have overall greater values in their stepwise connectivity amyloid maps than patients with Alzheimer's disease. However, this is not the case. When using the same absolute *z*-score value threshold, the Alzheimer's disease group shows greater values in the stepwise connectivity amyloid maps than elderly controls (Supplementary Fig. 3).

The earliest stage of the amyloid network in the elderly brain

To confirm that the midline prefrontal and orbitofrontal cortex are dominant regions in early stages of the amyloid-β network, we performed additional analyses using only elderly controls with low amyloid-β burden. First, our stepwise connectivity analysis of HFPG reveals direct associations with the ipsilateral (Fig. 4Aa) and contralateral amygdala and anterior hippocampus (detailed inset in Fig. 4A). There are no direct associations with any cortical structure (one link-step map to HFPG; Fig. 4A). In further link-step distances (two and three link-step maps to HFPG; Fig. 4A) we found an association between amyloid-β deposits in HFPG, amygdala nucleus (Fig. 4Ab and d) and orbitofrontal cortex (Fig. 4Ac and e), as well as a subtle association with cingulum areas (Fig. 4Af) (see also Supplementary Fig. 4 for a replication of this finding in an independent data set of elderly controls with low amyloid-β burden).

Amyloid hubs and longitudinal changes

Finally, we focus our attention on the network hubs and the longitudinal changes that occur in elderly controls with low amyloid-β burden. We postulate that regions that exhibit a high degree of spatial amyloid-β co-variation with other regions in early stages may be related to brain mechanisms underlying amyloid-β spreading. First, we study longitudinal changes in the elderly controls with low amyloid-β burden. We found that HFPG shows significant changes in direct spatial associations with the lateral temporal lobes (Fig. 4Ba), precuneus and contralateral HFPG and amygdala nucleus (Fig. 4Bb) after 1 year of follow-up. This finding suggests that once amyloid-β accumulation has begun in the amygdala-orbitofrontal-HFPG triplet then a more lateral and posterior brain

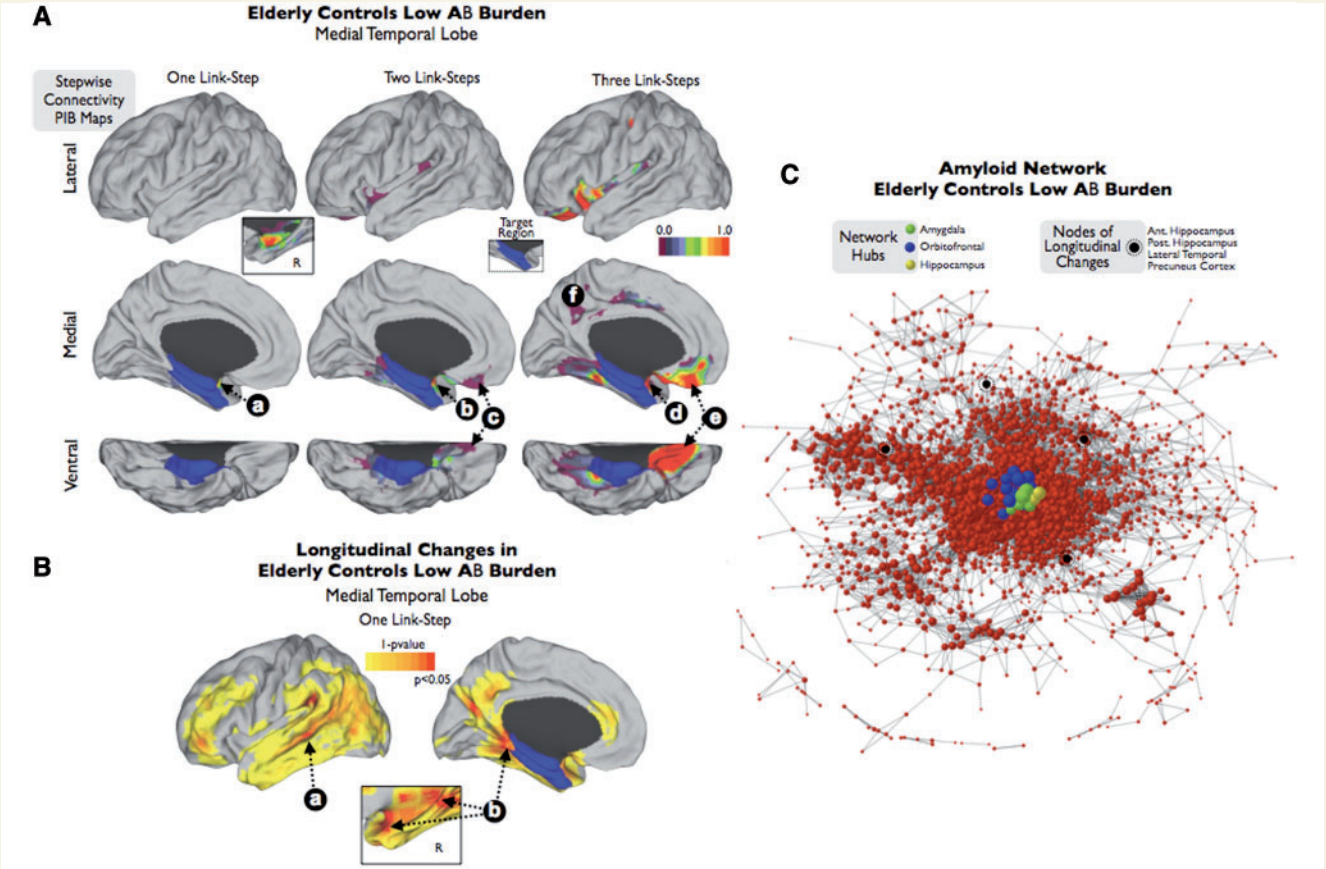

Figure 4 Stepwise connectivity analysis of medial temporal lobe (**A** and **B**) and visualization of the amyloid network (**C**) in elderly controls with very low amyloid-β burden. Inset in **A** shows the contra-lateral amyloid-β connectivity in one-step. In the network graph (**C**), size of nodes represents degree centrality values (larger nodes denote high number of connections to the rest of the network). Colour bars represent normalized *z*-score scale in **A**; and 1 minus *P*-value scale in **B**.

pattern of progression emerges. It is important to note that a more conventional statistical analysis to compare the baseline and follow-up PIB-distribution volume ratio maps (Supplementary Fig. 5), such as a paired *t*-test, did not show significant differences. Second, in order to quantify the network centrality or hub property of brain regions at the early stages of amyloid-β pathology, we ranked all grey matter regions based on the degree centrality value in the amyloid-β association network of the elderly PIB-negative group. We found that the amygdala nucleus and orbitofrontal cortex, and to a less extent the anterior hippocampus, are the most important hubs of the amyloid-β association network of the elderly PIB-negative group (Table 2). Accordingly, these three brain regions exhibit a central position in the graph (Fig. 4C, shows the network location of the top 20 hubs from Table 2 in different colours) and nodes that show longitudinal changes in the follow-up, such as the posterior hippocampus, lateral temporal, ventrolateral prefrontal or precuneus cortices (Fig. 4B) are placed in the periphery of the graph (dark nodes in Fig. 4C). Third, we compare the PIB-distribution volume ratio intensity and mean degree centrality values (normalized and non-normalized by the total amount of brain degree) in the medial temporal lobe of the study groups. As shown in Supplementary Fig. 6, PIB-distribution volume ratio intensity and degree centrality reflect different types of information. For instance, elderly controls with low amyloid-β burden have lower PIB-distribution volume ratio intensity values compared with patients with Alzheimer's disease, but the highest normalized degree of connectivity. This suggests that in early stages of amyloid deposition it may be more relevant to study the co-variation with the medial temporal lobe rather than its absolute PIB-distribution volume ratio intensity.

Table 2 Top degree centrality values of grey matter nodes in the network of elderly subjects with very low amyloid-β burden

Region	MNI (*x*, *y*, *z*)	Degree value
Amygdala nucleus (R)	30, 8, −10	65
Amygdala nucleus (R)	30, 0, −10	52
Orbitofrontal cortex (L)	−18, 24, −18	50
Orbitofrontal cortex (L)	−18, 16, −10	50
Orbitofrontal cortex (L)	−10, 24, −18	48
Hippocampus (L)	34, −8, −10	44
Orbitofrontal cortex (L)	−10, 32, −18	43
Amygdala nucleus (L)	−26, 0, −10	42
Orbitofrontal cortex (L)	−18, 24, −26	40
Orbitofrontal cortex (L)	−18, 32, −18	38
Amygdala nucleus (R)	22, 8, −10	37
Amygdala nucleus (L)	−26, 8, −10	37
Orbitofrontal cortex (R)	22, 16, −10	37
Orbitofrontal cortex (L)	−18, 16, −18	35
Orbitofrontal cortex (R)	6, 32, −18	35
Orbitofrontal cortex (L)	−26, 24, −10	35
Orbitofrontal cortex (L)	− 2, 32, −18	33
Hippocampus (L)	−34, −16, −10	33
Orbitofrontal cortex (L)	−10, 40, −2	32
Orbitofrontal cortex (L)	−10, 16, −18	31

Discussion

Cognitively normal individuals with elevated levels of brain amyloid-β have a high risk of developing symptomatic Alzheimer's disease in the upcoming years (Morris *et al*., 2009; Jack *et al*., 2010; Sperling *et al*., 2011). Several studies have shown that preclinical stages of Alzheimer's disease, by virtue of high amyloid-β accumulation, suffer from early brain functional and structural changes that might be critical to understanding the transition to symptomatic forms of Alzheimer's disease-related neurodegeneration (Hedden *et al*., 2009; Sperling *et al*., 2009, 2011; Becker *et al*., 2011). However, even at very early stages of amyloid-β deposition, for example in those subjects classified as amyloid-β negative based on current PIB-PET standards, it is possible to detect meaningful patterns of brain changes that suggest an eventual development of Alzheimer's disease-related pathology (Villain *et al*., 2012). In this sense, amyloid-β accumulation in the human brain is not a static phenomenon but a progression, likely starting during the asymptomatic period (Sabuncu *et al*., 2011, 2012; Sojkova *et al*., 2011; Villemagne *et al*., 2011; Vlassenko *et al*., 2011) and advancing along neural networks (Pearson and Powell, 1989; Seeley *et al*., 2009) until reaching the Alzheimer's disease phase (Jack *et al*., 2009, 2010). Our findings support this view. We studied the connectivity relationships between local brain systems such as the medial temporal lobe and distributed systems, such as key regions of the default mode network, in order to characterize the connectional fingerprints of neurodegeneration and potential pathways where amyloid-β expands. We show that amyloid-β associations between brain regions, rather than the amyloid-β accumulation in terms of PIB-distribution volume ratio intensity (Supplementary Fig. 5), seem to track key features of Alzheimer's pathology. Analyses of elderly controls with low amyloid-β burden show that there are predominant associations between amyloid-β deposits in the medial temporal lobe, orbitofrontal cortex and amygdala. In fact, these regions represent the core hubs of the amyloid-β network. On the other hand, it is the peripheral nodes of the amyloid-β network that progress over time. These findings suggest that very early network axes of pathology may exist (green nodes in Fig. 5) from amyloid-β hubs to peripheral network regions such as temporal, frontal and parietal areas (blue nodes in Fig. 5). In this sense, our results may provide some clues regarding where fibrillar amyloid-β starts accumulating in the human brain and expands as the disease progresses.

Alzheimer's disease is a network disease

For several decades, it has been postulated that the pathological changes in Alzheimer's disease affect and extend through interconnected neurons (Saper *et al*., 1987; Pearson and Powell, 1989). In other words, the pattern of distribution of neurofibrillary tangles and neuritic plaques has pointed out that Alzheimer's disease-related brain changes are strongly associated with anatomical interconnectivity (Pearson and Powell, 1989; Arnold *et al*., 1991; Braak and Braak, 1991*b*). After this line of research and congruent

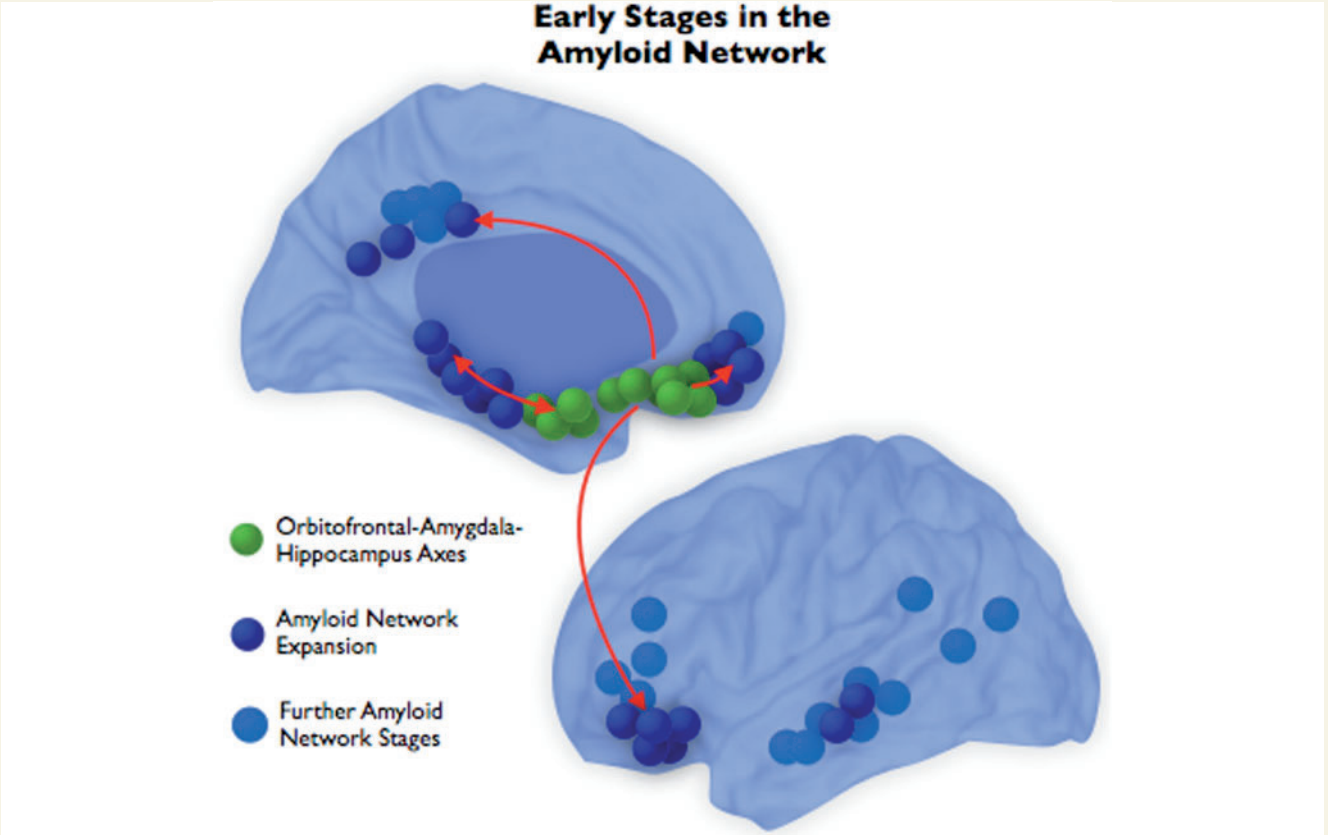

Figure 5 Based on our findings from elderly control subjects with low amyloid-β accumulation, we postulate that amyloid-β initially expands from the amygdala-orbitofrontal-hippocampal formation to the posterior medial and lateral temporal lobe and the midline and lateral frontal lobe.

with previous observations, several recent investigations have found that Alzheimer's disease-related neurodegeneration follows specific functional connectivity or metabolic networks of the human brain such as the default mode network (Seeley *et al*., 2009; Villain *et al*., 2010; Raj *et al*., 2012; Zhou *et al*., 2012). It is now well known that default mode network regions are preferentially vulnerable to amyloid-β deposition (Klunk *et al*., 2004; Buckner *et al*., 2008), increase of glycolysis (Vlassenko *et al*., 2010) and disruption of activity and metabolism (Minoshima *et al*., 1997; Lustig *et al*., 2003; Greicius *et al*., 2004). In this sense, these studies have introduced a renewed enthusiasm about the network nature of Alzheimer's disease, leading to a new reformulation of the Hebbian principle that 'not only neurons that fire together wire together (Hebb, 1961) but also neurons that wire together die together' (Sepulcre *et al*., 2012*a*).

In the era of neuroimaging, two viewpoints have shaped the landscape of Alzheimer's disease research: one focused on the hippocampus degeneration and the other on the large-scale disruption of the default mode network. However, Alzheimer's disease studies have sometimes been inconsistent and it has been difficult to reconcile the default mode network findings with more local HFPG degeneration. A striking example is the postulation that high basal and sustained metabolism is a key factor to developing amyloid-β deposition. This is in contrast with the observations that the hippocampal formation, an early affected region, does not show high functional connectivity or metabolic activity and it is not a central functional hub in the normal human brain (Buckner *et al*., 2009; Royall, 2010). One explanation for this inconsistency may be the characteristic features of HFPG, which show preferential affinity for neurofibrillary tangle or paired helical filament tauopathy but not for high neurtic plaques/amyloid-β deposits (Mann, 1985; Pearson and Powell, 1989; Arnold *et al*., 1991; Braak and Braak, 1991*b*). As has been shown before, early stages of Alzheimer's disease show a low density of amyloid-β in HFPG, which is mostly concentrated in the presubiculum and entorhinal cortex, but overall much less than other regions such as the temporal rostral or orbitofrontal cortices (Braak and Braak, 1991*b*). In this sense, several researchers have postulated that the HFPG may make a key contribution in the neurodegeneration process by first intraneuronally accumulating neurofibrillary tangles and second extraneuronally inducing amyloid-β deposition in its synaptic terminals of projecting neurons (Pearson and Powell, 1989). This view accounts for the mismatch between neurofibrillary tangle and amyloid-β deposits in HFPG and predicts that from just a few neurofibrillary tangle-affected neurons it is possible to generate a high number of amyloid-β deposits in its efferent targets, especially orbitofrontal cortex and other medial temporal regions. An alternative explanation is that rather than the total amount of amyloid-β accumulated in the HFPG, its co-variation with deposits in the rest of the brain

might be more important. This idea is partially supported by our data. HFPG has meaningful amyloid-β deposits that highly co-vary within the contra-lateral HFPG and with external distributed regions such as orbitofrontal, lateral temporal and posterior cingulate cortex/precuneus cortices in Alzheimer's disease and elderly controls. In other words, HFPG and central regions of the default mode network are indeed highly related in terms of amyloid-β accumulation independently of the different amount of absolute regional deposition.

The amygdala-hippocampus-orbitofrontal triplet in the early stages of amyloid-β deposition

Recent data shows that there is a continuous accumulation of amyloid-β protein from healthy ageing to Alzheimer's disease, where higher amyloid-β burden at baseline is associated with higher amyloid-β deposition in the future (Jack *et al*., 2009; Sojkova *et al*., 2011; Villemagne *et al*., 2011; Villain *et al*., 2012). However, the details of this continuum remain elusive; for instance, how and where does amyloid-β start its accumulation in the normal brain or does the accumulation reach a plateau when cognitive decline appears, especially, at the Alzheimer's disease stage (Andreasen *et al*., 1999; Engler *et al*., 2006; Grimmer *et al*., 2010; Jack *et al*., 2010; Petersen, 2010; Kadir *et al*., 2011; Koivunen *et al*., 2011; Sperling *et al*., 2011; Villemagne *et al*., 2011; Weiner *et al*., 2012). As part of one characterization of the early phases of amyloid-β accumulation, Villain *et al*. (2012) describe that, in PIB negative individuals, it is possible to detect meaningful longitudinal changes in the temporo-parietal junction and the posterior cingulate cortex. Our study also provides novel findings related to the low amyloid-β burden population, although in another direction. We found that the amygdala, orbitofrontal cortex and HFPG form a robust triplet of amyloid-β connectivity that seems to have a central role in the preclinical pathological network. We described an anterior pattern of connectivity between the medial temporal and the frontal lobe in low amyloid-β healthy controls that may represent a putative pathway for the spreading of pathology and lead to a future conversion to Alzheimer's disease. It is important to remark here that our hub measure captures the extent of the association between a given region and the rest of the brain. If only few specific regions display hub properties, then it is plausible to think that they may represent centres of vulnerability. Our first hypothesis was that the HFPG could be the top hub in the amyloid-β network, however, the amygdala and orbitofrontal cortex turn out to have a higher 'hubness' in the early amyloid-β network computed on healthy elderly subjects with low amyloid-β burden. The posterior hippocampus, posterior cingulate cortex, and temporo-parietal junction seem to make an important contribution in the longitudinal progression during the very early stages of amyloid-β accumulation.

The spreading of Alzheimer's disease

Alzheimer's disease has been consistently postulated as spreading through long-range connections in the brain rather than a proximity-wise progression (Pearson and Powell, 1989; Arnold *et al*., 1991; Braak and Braak, 1991*b*). More recent findings using high-resolution neuroimaging techniques and animal models seem to confirm some of the principles formulated in the past (Seeley *et al*., 2009; de Calignon *et al*., 2012; Zhou *et al*., 2012). For instance, specific epicentres of the brain, such as default mode network-related regions, are likely to be the main venues by which the disease progresses in the brain (Raj *et al*., 2012; Zhou *et al*., 2012). At the molecular level, it is likely that transneuronal spread in a 'prion-like' manner or other transaxonal/transsynaptic propagation mechanisms take place during the progression of amyloid-β and tau (Buxbaum *et al*., 1998; Lazarov *et al*., 2002; de Calignon *et al*., 2012; Walker *et al*., 2012). Our study does not clarify the spreading mechanisms or causal associations between affected regions in Alzheimer's disease but shows connectional fingerprints with high potential of being pathological-related and part of spreading pathways. For instance, the amyloid-β network of healthy low amyloid burden individuals shows that the amygdala nucleus, orbitofrontal cortex and hippocampus have a hub role in the network configuration, but it is mostly the peripheral nodes of the network that experience expansion over time. This finding supports the plausible interpretation of amyloid-β pathology advancing through a connected network of regions. This view also suggests that the hub regions in the amyloid-β network of healthy low amyloid burden individuals are likely to be plausible candidates where the amyloid-β pathology originally started. Hence, it seems that the triplet of amygdala nucleus, orbitofrontal cortex and HFPG, but especially the amygdala nucleus, may be the beginning of Alzheimer's disease-related amyloid-β alterations and the gateway to distributed cortical systems in the brain such as the default mode network. Interestingly, previous research has also suggested that the amygdala may be involved in the spreading process of the disease due to the reciprocal connections and matching numbers of tangles between the amygdala and key Alzheimer's disease-related regions of the neocortex (Esiri *et al*., 1990). The fact that amyloid-β accumulation in both HFPG and orbitofrontal cortex are primarily connected to the amygdala and that the amygdala is the top hub in the amyloid-β network, reminds previous interest of amygdala in Alzheimer's disease. The amygdala nucleus has been found to be severely affected in Alzheimer's disease (Herzog and Kemper, 1980; Esiri *et al*., 1990; Kromer Vogt *et al*., 1990; Poulin *et al*., 2011) and has been postulated as one of the central regions for early amyloid-β changes (Mann *et al*., 1987), although not necessarily a region with high amyloid-β binding. Moreover, the amygdala has key connectivity to the nucleus basalis of Meynert (Mesulam and Mufson, 1984; Palmer *et al*., 1986), the degeneration of which might explain the neocortical cholinergic deficits present in Alzheimer's disease (Francis *et al*., 1987; Esiri *et al*., 1990).

Conclusions and limitations

The emerging tools of what is called 'network medicine' offer a platform to study complex systems in neuroscience and uncover the biological mechanisms of neurological disorders (Sporns *et al*., 2004; Bullmore and Sporns, 2009; Barabasi *et al*., 2011). Network techniques applied to neuroimaging data present the attractive

possibility of improving our understanding of the disease, while providing us with better capability of staging individuals at risk of Alzheimer's disease. Our study has some limitations that need to be indicated. First, we must acknowledge that our study considers brain amyloidosis as a central neuropathological event in Alzheimer's disease, and, therefore, we are only investigating a portion of the complex tissue alterations that take place in the disease (for instance tau or non-fibrillar amyloid-β accumulations). Secondly, we found some discrepancies between the amyloid-β and functional connectivity MRI connectivity maps of patients with Alzheimer's disease and young control subjects. It is likely that other factors and not just the functional pathways of the brain play a role in the spreading distribution of the amyloid-β pathology. Finally, our network analyses based on linear statistical inferences do not provide directionality information about the relationships between regions and are not suitable for drawing conclusions regarding causation.

Acknowledgements

We like to thank the helpful comments of William Seeley and Michael Greicius at the initial stages of this project. We thank Randy L. Buckner for generously providing the functional connectivity MRI data of the young control group and also for his valuable comments to the study. We thank the investigators and staff of the Massachusetts Alzheimer's Disease Research Center (ADRC), the individual research participants, and their families and caregivers. We like to thank the PET Core of the MGH, the Harvard Centre for Brain Science Neuroimaging Core and the Athinoula A. Martinos Centre for imaging support.

Funding

This research was supported by grants from the US National Institute of Health (NIH) (K25EB013649-01 to M.R.S.; R01-AG027435-S1 to R.A.S. and K.A.J.; Harvard Aging Brain Study: P01-AG036694 to R.A.S and K.A.J.; Massachusetts ADRC: P50-AG00513421 to K.A.J. and R.A.S.) and Alzheimer's Association (NIRG-11-205690 to J.S.; IIRG-06-32444 to R.A.S. and K.A.J.; ZEN-10-174210 to K.A.J.).

Supplementary material

Supplementary material is available at *Brain* online.

References

Andreasen N, Hesse C, Davidsson P, Minthon L, Wallin A, Winblad B, et al. Cerebrospinal fluid beta-amyloid(1-42) in Alzheimer disease: differences between early- and late-onset Alzheimer disease and stability during the course of disease. Arch Neurol 1999; 56: 673–80.

Arnold SE, Hyman BT, Flory J, Damasio AR, Van Hoesen GW. The topographical and neuroanatomical distribution of neurofibrillary tangles and neuritic plaques in the cerebral cortex of patients with Alzheimer's disease. Cereb Cortex 1991; 1: 103–16.

Bacskai BJ, Hickey GA, Skoch J, Kajdasz ST, Wang Y, Huang GF, et al. Four-dimensional multiphoton imaging of brain entry, amyloid binding, and clearance of an amyloid-beta ligand in transgenic mice. Proc Natl Acad Sci USA 2003; 100: 12462–7.

Barabasi AL, Gulbahce N, Loscalzo J. Network medicine: a network-based approach to human disease. Nat Rev Genet 2011; 12: 56–68.

Becker JA, Hedden T, Carmasin J, Maye J, Rentz DM, Putcha D, et al. Amyloid-beta associated cortical thinning in clinically normal elderly. Ann Neurol 2011; 69: 1032–42.

Benjamini Y, Hochberg Y. Controlling the false discovery rate: a practical and powerful approach to multiple testing. J R Statist Soc 1995; 57: 289–300.

Bero AW, Bauer AQ, Stewart FR, White BR, Cirrito JR, Raichle ME, et al. Bidirectional relationship between functional connectivity and amyloid-beta deposition in mouse brain. J Neurosci 2012; 32: 4334–40.

Bero AW, Yan P, Roh JH, Cirrito JR, Stewart FR, Raichle ME, et al. Neuronal activity regulates the regional vulnerability to amyloid-beta deposition. Nat Neurosci 2011; 14: 750–6.

Birn RM, Diamond JB, Smith MA, Bandettini PA. Separating respiratory-variation-related fluctuations from neuronal-activity-related fluctuations in fMRI. Neuroimage 2006; 31: 1536–48.

Biswal B, Yetkin FZ, Haughton VM, Hyde JS. Functional connectivity in the motor cortex of resting human brain using echo-planar MRI. Magn Reson Med 1995; 34: 537–41.

Braak H, Alafuzoff I, Arzberger T, Kretzschmar H, Del Tredici K. Staging of Alzheimer disease-associated neurofibrillary pathology using paraffin sections and immunocytochemistry. Acta Neuropathol 2006; 112: 389–404.

Braak H, Braak E. Demonstration of amyloid deposits and neurofibrillary changes in whole brain sections. Brain Pathol 1991a; 1: 213–6.

Braak H, Braak E. Neuropathological stageing of Alzheimer-related changes. Acta Neuropathol 1991b; 82: 239–59.

Braak H, Braak E, Ohm T, Bohl J. Alzheimer's disease: mismatch between amyloid plaques and neuritic plaques. Neurosci Lett 1989; 103: 24–8.

Brody DL, Magnoni S, Schwetye KE, Spinner ML, Esparza TJ, Stocchetti N, et al. Amyloid-beta dynamics correlate with neurological status in the injured human brain. Science 2008; 321: 1221–4.

Buckner RL, Andrews-Hanna JR, Schacter DL. The brain's default network: anatomy, function, and relevance to disease. Ann N Y Acad Sci 2008; 1124: 1–38.

Buckner RL, Sepulcre J, Talukdar T, Krienen FM, Liu H, Hedden T, et al. Cortical hubs revealed by intrinsic functional connectivity: mapping, assessment of stability, and relation to Alzheimer's disease. J Neurosci 2009; 29: 1860–73.

Bullmore E, Sporns O. Complex brain networks: graph theoretical analysis of structural and functional systems. Nat Rev Neurosci 2009; 10: 186–98.

Buxbaum JD, Thinakaran G, Koliatsos V, O'Callahan J, Slunt HH, Price DL, et al. Alzheimer amyloid protein precursor in the rat hippocampus: transport and processing through the perforant path. J Neurosci 1998; 18: 9629–37.

Cirrito JR, Yamada KA, Finn MB, Sloviter RS, Bales KR, May PC, et al. Synaptic activity regulates interstitial fluid amyloid-beta levels in vivo. Neuron 2005; 48: 913–22.

de Calignon A, Polydoro M, Suarez-Calvet M, William C, Adamowicz DH, Kopeikina KJ, et al. Propagation of tau pathology in a model of early Alzheimer's disease. Neuron 2012; 73: 685–97.

de Nooy W, Mrvar A, Batageli V. Exploratory social network analysis with Pajek. Cambridge: Cambridge University Press, 2005.

Engler H, Forsberg A, Almkvist O, Blomquist G, Larsson E, Savitcheva I, et al. Two-year follow-up of amyloid deposition in patients with Alzheimer's disease. Brain 2006; 129: 2856–66.

Esiri MM, Pearson RC, Steele JE, Bowen DM, Powell TP. A quantitative study of the neurofibrillary tangles and the choline acetyltransferase activity in the cerebral cortex and the amygdala in Alzheimer's disease. J Neurol Neurosurg Psychiatry 1990; 53: 161–5.

Forsberg A, Engler H, Almkvist O, Blomquist G, Hagman G, Wall A, et al. PET imaging of amyloid deposition in patients with mild cognitive impairment. Neurobiol Aging 2008; 29: 1456–65.

Francis PT, Carl R, Pearson A, Lowe SL, Neal JW, Stephens PH, et al. The dementia of Alzheimer's disease: an update. J Neurol Neurosurg Psychiatry 1987; 50: 242–3.

Gomperts SN, Rentz DM, Moran E, Becker JA, Locascio JJ, Klunk WE, et al. Imaging amyloid deposition in Lewy body diseases. Neurology 2008; 71: 903–10.

Gouras GK, Relkin NR, Sweeney D, Munoz DG, Mackenzie IR, Gandy S. Increased apolipoprotein E epsilon 4 in epilepsy with senile plaques. Ann Neurol 1997; 41: 402–4.

Greicius M. Resting-state functional connectivity in neuropsychiatric disorders. Curr Opin Neurol 2008; 21: 424–30.

Greicius MD, Srivastava G, Reiss AL, Menon V. Default-mode network activity distinguishes Alzheimer's disease from healthy aging: evidence from functional MRI. Proc Natl Acad Sci USA 2004; 101: 4637–42.

Grimmer T, Tholen S, Yousefi BH, Alexopoulos P, Forschler A, Forstl H, et al. Progression of cerebral amyloid load is associated with the apolipoprotein E epsilon4 genotype in Alzheimer's disease. Biol Psychiatry 2010; 68: 879–84.

Gusnard DA, Raichle ME. Searching for a baseline: functional imaging and the resting human brain. Nat Rev Neurosci 2001; 2: 685–94.

Hardy J. An 'anatomical cascade hypothesis' for Alzheimer's disease. Trends Neurosci 1992; 15: 200–1.

Hardy JA, Higgins GA. Alzheimer's disease: the amyloid cascade hypothesis. Science 1992; 256: 184–5.

Hebb DO. Distinctive features of learning in the higher animal. London: Oxford University Press, 1961.

Hedden T, Van Dijk KR, Becker JA, Mehta A, Sperling RA, Johnson KA, et al. Disruption of functional connectivity in clinically normal older adults harboring amyloid burden. J Neurosci 2009; 29: 12686–94.

Herzog AG, Kemper TL. Amygdaloid changes in aging and dementia. Arch Neurol 1980; 37: 625–9.

Hughes CP, Berg L, Danziger WL, Coben LA, Martin RL. A new clinical scale for the staging of dementia. Br J Psychiatry 1982; 140: 566–72.

Hyman BT, Phelps CH, Beach TG, Bigio EH, Cairns NJ, Carrillo MC, et al. National Institute on Aging-Alzheimer's Association guidelines for the neuropathologic assessment of Alzheimer's disease. Alzheimers Dement 2012; 8: 1–13.

Hyman BT, Van Hoesen GW, Damasio AR, Barnes CL. Alzheimer's disease: cell-specific pathology isolates the hippocampal formation. Science 1984; 225: 1168–70.

Ikonomovic MD, Klunk WE, Abrahamson EE, Mathis CA, Price JC, Tsopelas ND, et al. Post-mortem correlates of in vivo PIB-PET amyloid imaging in a typical case of Alzheimer's disease. Brain 2008; 131: 1630–45.

Jack CR Jr, Knopman DS, Jagust WJ, Shaw LM, Aisen PS, Weiner MW, et al. Hypothetical model of dynamic biomarkers of the Alzheimer's pathological cascade. Lancet Neurol 2010; 9: 119–28.

Jack CR Jr, Lowe VJ, Weigand SD, Wiste HJ, Senjem ML, Knopman DS, et al. Serial PIB and MRI in normal, mild cognitive impairment and Alzheimer's disease: implications for sequence of pathological events in Alzheimer's disease. Brain 2009; 132: 1355–65.

Johnson KA, Gregas M, Becker JA, Kinnecom C, Salat DH, Moran EK, et al. Imaging of amyloid burden and distribution in cerebral amyloid angiopathy. Ann Neurol 2007; 62: 229–34.

Kadir A, Marutle A, Gonzalez D, Scholl M, Almkvist O, Mousavi M, et al. Positron emission tomography imaging and clinical progression in relation to molecular pathology in the first Pittsburgh Compound B positron emission tomography patient with Alzheimer's disease. Brain 2011; 134: 301–17.

Kalus P, Braak H, Braak E, Bohl J. The presubicular region in Alzheimer's disease: topography of amyloid deposits and neurofibrillary changes. Brain Res 1989; 494: 198–203.

Kamada T, Kawai S. An algorithm for drawing general undirected graphs information processing letters1989; 31: 7–15.

Kamenetz F, Tomita T, Hsieh H, Seabrook G, Borchelt D, Iwatsubo T, et al. APP processing and synaptic function. Neuron 2003; 37: 925–37.

Kemppainen NM, Aalto S, Wilson IA, Nagren K, Helin S, Bruck A, et al. PET amyloid ligand [11C]PIB uptake is increased in mild cognitive impairment. Neurology 2007; 68: 1603–6.

Klunk WE, Engler H, Nordberg A, Wang Y, Blomqvist G, Holt DP, et al. Imaging brain amyloid in Alzheimer's disease with Pittsburgh Compound-B. Ann Neurol 2004; 55: 306–19.

Klunk WE, Wang Y, Huang GF, Debnath ML, Holt DP, Mathis CA. Uncharged thioflavin-T derivatives bind to amyloid-beta protein with high affinity and readily enter the brain. Life Sci 2001; 69: 1471–84.

Koivunen J, Scheinin N, Virta JR, Aalto S, Vahlberg T, Nagren K, et al. Amyloid PET imaging in patients with mild cognitive impairment: a 2-year follow-up study. Neurology 2011; 76: 1085–90.

Kromer Vogt LJ, Hyman BT, Van Hoesen GW, Damasio AR. Pathological alterations in the amygdala in Alzheimer's disease. Neuroscience 1990; 37: 377–85.

Lazarov O, Lee M, Peterson DA, Sisodia SS. Evidence that synaptically released beta-amyloid accumulates as extracellular deposits in the hippocampus of transgenic mice. J Neurosci 2002; 22: 9785–93.

Lewis DA, Campbell MJ, Terry RD, Morrison JH. Laminar and regional distributions of neurofibrillary tangles and neuritic plaques in Alzheimer's disease: a quantitative study of visual and auditory cortices. J Neurosci 1987; 7: 1799–808.

Logan J, Fowler JS, Volkow ND, Wolf AP, Dewey SL, Schlyer DJ, et al. Graphical analysis of reversible radioligand binding from time-activity measurements applied to [N-11C-methyl]-(-)-cocaine PET studies in human subjects. J Cereb Blood Flow Metab 1990; 10: 740–7.

Lopresti BJ, Klunk WE, Mathis CA, Hoge JA, Ziolko SK, Lu X, et al. Simplified quantification of Pittsburgh Compound B amyloid imaging PET studies: a comparative analysis. J Nucl Med 2005; 46: 1959–72.

Lustig C, Snyder AZ, Bhakta M, O'Brien KC, McAvoy M, Raichle ME, et al. Functional deactivations: change with age and dementia of the Alzheimer type. Proc Natl Acad Sci USA 2003; 100: 14504–9.

Mackenzie IR, Miller LA. Senile plaques in temporal lobe epilepsy. Acta Neuropathol 1994; 87: 504–10.

Mann DM. The neuropathology of Alzheimer's disease: a review with pathogenetic, aetiological and therapeutic considerations. Mech Ageing Dev 1985; 31: 213–55.

Mann DM, Tucker CM, Yates PO. The topographic distribution of senile plaques and neurofibrillary tangles in the brains of non-demented persons of different ages. Neuropathol Appl Neurobiol 1987; 13: 123–39.

Mathis CA, Bacskai BJ, Kajdasz ST, McLellan ME, Frosch MP, Hyman BT, et al. A lipophilic thioflavin-T derivative for positron emission tomography (PET) imaging of amyloid in brain. Bioorg Med Chem Lett 2002; 12: 295–8.

Mathis CA, Wang Y, Holt DP, Huang GF, Debnath ML, Klunk WE. Synthesis and evaluation of 11C-labeled 6-substituted 2-arylbenzothiazoles as amyloid imaging agents. J Med Chem 2003; 46: 2740–54.

Mattson MP. Pathways towards and away from Alzheimer's disease. Nature 2004; 430: 631–9.

McKhann G, Drachman D, Folstein M, Katzman R, Price D, Stadlan EM. Clinical diagnosis of Alzheimer's disease: report of the NINCDS-ADRDA Work Group under the auspices of Department of Health and Human Services Task Force on Alzheimer's Disease. Neurology 1984; 34: 939–44.

Mesulam MM, Mufson EJ. Neural inputs into the nucleus basalis of the substantia innominata (Ch4) in the rhesus monkey. Brain 1984; 107 (Pt 1): 253–74.

Minoshima S, Giordani B, Berent S, Frey KA, Foster NL, Kuhl DE. Metabolic reduction in the posterior cingulate cortex in very early Alzheimer's disease. Ann Neurol 1997; 42: 85–94.

Mintun MA, Larossa GN, Sheline YI, Dence CS, Lee SY, Mach RH, et al. [11C]PIB in a nondemented population: potential antecedent marker of Alzheimer disease. Neurology 2006; 67: 446–52.

Morris JC. The Clinical Dementia Rating (CDR): current version and scoring rules. Neurology 1993; 43: 2412–4.

Morris JC, Roe CM, Grant EA, Head D, Storandt M, Goate AM, et al. Pittsburgh Compound B imaging and prediction of progression from cognitive normality to symptomatic Alzheimer disease. Arch Neurol 2009; 66: 1469–75.

Nitsch RM, Farber SA, Growdon JH, Wurtman RJ. Release of amyloid beta-protein precursor derivatives by electrical depolarization of rat hippocampal slices. Proc Natl Acad Sci USA 1993; 90: 5191–3.

Nordberg A. PET imaging of amyloid in Alzheimer's disease. Lancet Neurol 2004; 3: 519–27.

Ogomori K, Kitamoto T, Tateishi J, Sato Y, Suetsugu M, Abe M. Beta-protein amyloid is widely distributed in the central nervous system of patients with Alzheimer's disease. Am J Pathol 1989; 134: 243–51.

Palmer AM, Procter AW, Stratmann GC, Bowen DM. Excitatory amino acid-releasing and cholinergic neurones in Alzheimer's disease. Neurosci Lett 1986; 66: 199–204.

Palop JJ, Chin J, Mucke L. A network dysfunction perspective on neurodegenerative diseases. Nature 2006; 443: 768–73.

Palop JJ, Mucke L. Amyloid-beta-induced neuronal dysfunction in Alzheimer's disease: from synapses toward neural networks. Nat Neurosci 2010; 13: 812–8.

Pearson RC, Powell TP. The neuroanatomy of Alzheimer's disease. Rev Neurosci 1989; 2: 101–22.

Petersen RC. Alzheimer's disease: progress in prediction. Lancet Neurol 2010; 9: 4–5.

Poulin SP, Dautoff R, Morris JC, Barrett LF, Dickerson BC. Amygdala atrophy is prominent in early Alzheimer's disease and relates to symptom severity. Psychiatry Res 2011; 194: 7–13.

Raj A, Kuceyeski A, Weiner M. A network diffusion model of disease progression in dementia. Neuron 2012; 73: 1204–15.

Rentz DM, Locascio JJ, Becker JA, Moran EK, Eng E, Buckner RL, et al. Cognition, reserve, and amyloid deposition in normal aging. Ann Neurol 2010; 67: 353–64.

Rowe CC, Ng S, Ackermann U, Gong SJ, Pike K, Savage G, et al. Imaging beta-amyloid burden in aging and dementia. Neurology 2007; 68: 1718–25.

Royall DR. A Tangled Web (eLetters). J Neurosci 2010; 29: 1860–73.

Sabuncu MR, Buckner RL, Smoller JW, Lee PH, Fischl B, Sperling RA. The association between a polygenic Alzheimer score and cortical thickness in clinically normal subjects. Cereb Cortex 2012; 22: 2653–61.

Sabuncu MR, Desikan RS, Sepulcre J, Yeo BT, Liu H, Schmansky NJ, et al. The dynamics of cortical and hippocampal atrophy in Alzheimer disease. Arch Neurol 2011; 68: 1040–8.

Saper CB, Wainer BH, German DC. Axonal and transneuronal transport in the transmission of neurological disease: potential role in system degenerations, including Alzheimer's disease. Neuroscience 1987; 23: 389–98.

Seeley WW, Crawford RK, Zhou J, Miller BL, Greicius MD. Neurodegenerative diseases target large-scale human brain networks. Neuron 2009; 62: 42–52.

Selkoe DJ. The ups and downs of Abeta. Nat Med 2006; 12: 758–9; discussion 759.

Sepulcre J, Liu H, Talukdar T, Martincorena I, Yeo BT, Buckner RL. The organization of local and distant functional connectivity in the human brain. PLoS Comput Biol 2010; 6: e1000808.

Sepulcre J, Sabuncu MR, Johnson KA. Network assemblies in the functional brain. Curr Opin Neurol 2012a; 25: 384–91.

Sepulcre J, Sabuncu MR, Yeo TB, Liu H, Johnson KA. Stepwise connectivity of the modal cortex reveals the multimodal organization of the human brain. J Neurosci 2012b; 32: 10649–61.

Sojkova J, Zhou Y, An Y, Kraut MA, Ferrucci L, Wong DF, et al. Longitudinal patterns of beta-amyloid deposition in nondemented older adults. Arch Neurol 2011; 68: 644–9.

Sperling RA, Aisen PS, Beckett LA, Bennett DA, Craft S, Fagan AM, et al. Toward defining the preclinical stages of Alzheimer's disease: recommendations from the National Institute on Aging-Alzheimer's Association workgroups on diagnostic guidelines for Alzheimer's disease. Alzheimers Dement 2011; 7: 280–92.

Sperling RA, Laviolette PS, O'Keefe K, O'Brien J, Rentz DM, Pihlajamaki M, et al. Amyloid deposition is associated with impaired default network function in older persons without dementia. Neuron 2009; 63: 178–88.

Sporns O, Chialvo DR, Kaiser M, Hilgetag CC. Organization, development and function of complex brain networks. Trends Cogn Sci 2004; 8: 418–25.

Thal DR, Rub U, Orantes M, Braak H. Phases of A beta-deposition in the human brain and its relevance for the development of AD. Neurology 2002; 58: 1791–800.

Tosun D, Schuff N, Mathis CA, Jagust W, Weiner MW. Spatial patterns of brain amyloid-beta burden and atrophy rate associations in mild cognitive impairment. Brain 2011; 134: 1077–88.

Tzourio-Mazoyer N, Landeau B, Papathanassiou D, Crivello F, Etard O, Delcroix N, et al. Automated anatomical labeling of activations in SPM using a macroscopic anatomical parcellation of the MNI MRI single-subject brain. Neuroimage 2002; 15: 273–89.

Van Dijk KR, Hedden T, Venkataraman A, Evans KC, Lazar SW, Buckner RL. Intrinsic functional connectivity as a tool for human connectomics: theory, properties, and optimization. J Neurophysiol 2010; 103: 297–321.

Van Essen DC, Dierker DL. Surface-based and probabilistic atlases of primate cerebral cortex. Neuron 2007; 56: 209–25.

Villain N, Chetelat G, Grassiot B, Bourgeat P, Jones G, Ellis KA, et al. Regional dynamics of amyloid-beta deposition in healthy elderly, mild cognitive impairment and Alzheimer's disease: a voxelwise PIB-PET longitudinal study. Brain 2012; 135 (Pt 7): 2126–39.

Villain N, Fouquet M, Baron JC, Mezenge F, Landeau B, de La Sayette V, et al. Sequential relationships between grey matter and white matter atrophy and brain metabolic abnormalities in early Alzheimer's disease. Brain 2010; 133: 3301–14.

Villemagne VL, Pike KE, Chetelat G, Ellis KA, Mulligan RS, Bourgeat P, et al. Longitudinal assessment of Abeta and cognition in aging and Alzheimer disease. Ann Neurol 2011; 69: 181–92.

Vlassenko AG, Mintun MA, Xiong C, Sheline YI, Goate AM, Benzinger TL, et al. Amyloid-beta plaque growth in cognitively normal adults: longitudinal [11C]Pittsburgh compound B data. Ann Neurol 2011; 70: 857–61.

Vlassenko AG, Vaishnavi SN, Couture L, Sacco D, Shannon BJ, Mach RH, et al. Spatial correlation between brain aerobic glycolysis and amyloid-beta (Abeta) deposition. Proc Natl Acad Sci USA 2010; 107: 17763–7.

Walker LC, Diamond MI, Duff KE, Hyman BT. Mechanisms of protein seeding in neurodegenerative diseases. Arch Neurol 2012; 10: 1–7.

Walsh DM, Selkoe DJ. Oligomers on the brain: the emerging role of soluble protein aggregates in neurodegeneration. Protein Pept Lett 2004; 11: 213–28.

Weiner MW, Veitch DP, Aisen PS, Beckett LA, Cairns NJ, Green RC, et al. The Alzheimer's disease neuroimaging initiative: a review of papers published since its inception. Alzheimers Dement 2012; 8: S1–68.

Yeo BT, Krienen FM, Sepulcre J, Sabuncu MR, Lashkari D, Hollinshead M, et al. The organization of the human cerebral cortex estimated by intrinsic functional connectivity. J Neurophysiol 2011; 106: 1125–65.

Zhou J, Gennatas ED, Kramer JH, Miller BL, Seeley WW. Predicting regional neurodegeneration from the healthy brain functional connectome. Neuron 2012; 73: 1216–27.